Thermodynamic Routes to Novel Metastable Nitrogen-Rich Nitrides

Wenhao Sun,[†,‡] Aaron Holder,[§,⊥] Bernardo Orvañanos,[‡] Elisabetta Arca,[§] Andriy Zakutayev,[§] Stephan Lany,[§] and Gerbrand Ceder*,[†,‡,∥]

[†]Materials Sciences Division, Lawrence Berkeley National Laboratory, Berkeley, California 94720, United States

[‡]Department of Materials Science and Engineering, Massachusetts Institute of Technology, Cambridge, Massachusetts 02139, United States

[§]National Renewable Energy Laboratory, Golden, Colorado 80401, United States

[∥]Department of Materials Science and Engineering, Univeristy of California, Berkeley, California 94720, United States

[⊥]Department of Chemical and Biological Engineering, Univeristy of Colorado, Boulder, Colorado 80309, United States

S *Supporting Information*

ABSTRACT: Compared to oxides, the nitrides are relatively unexplored, making them a promising chemical space for novel materials discovery. Of particular interest are nitrogen-rich nitrides, which often possess useful semiconducting properties for electronic and optoelectronic applications. However, such nitrogen-rich compounds are generally metastable, and the lack of a guiding theory for their synthesis has limited their exploration. Here, we review the remarkable metastability of observed nitrides, and examine the thermodynamics of how reactive nitrogen precursors can stabilize metastable nitrogen-rich compositions during materials synthesis. We map these thermodynamic strategies onto a predictive computational search, training a data-mined ionic substitution algorithm specifically for nitride discovery, which we combine with grand-canonical DFT-SCAN phase stability calculations to compute stabilizing nitrogen chemical potentials. We identify several new nitrogen-rich binary nitrides for experimental investigation, notably the transition metal nitrides Mn_3N_4, Cr_3N_4, V_3N_4, and Nb_3N_5, the main group nitride SbN, and the pernitrides FeN_2, CrN_2, and Cu_2N_2. By formulating rational thermodynamic routes to metastable compounds, we expand the search space for functional technological materials beyond equilibrium phases and compositions.
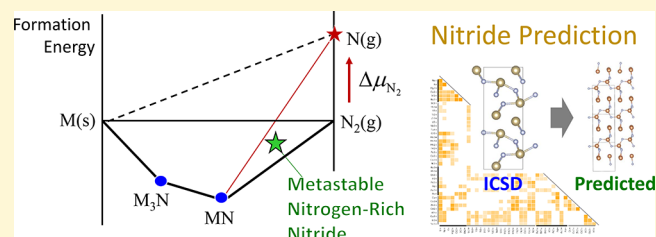
INTRODUCTION

High-throughput computational materials screening has become an established technique to efficiently probe for novel stable compositions across unexplored materials spaces.[1−6] These predicted compounds can focus the scope of experimental synthesis efforts, drastically accelerating materials exploration compared to traditional "Edisonian" trial-and-error searches.[7] Nitrides are a particularly compelling class of materials to explore computationally,[8−11] as they are rare in nature and difficult to synthesize in the laboratory. They also have significant technological relevance, as the unique bonding characteristics in nitrides yield electronic structures that range from metallic to semiconducting, producing materials with properties relevant to applications spanning refractory ceramics,[12,13] superconductors,[14,15] solid-state lighting,[16,17] photovoltaics,[18,19] photocatalysts,[20,21] thermoelectrics,[22,23] piezoelectrics,[24,25] permanent magnets,[26] and more.

Stability is a major search criterion in the computational discovery of new materials, and there is great emphasis placed on identifying ground-state materials. However, thermodynamically metastable phases are routinely observed during materials synthesis,[27,28] and may possess superior properties for some applications as compared to those of their corresponding

ground-states. If a metastable phase can be synthesized and kinetically retained, it can be a suitable candidate for use in functional devices. In nitrides, the low chemical reactivity of the N_2 molecule drives phase equilibrium toward nitrogen-poor compositions, typically leading to reduced nitrides with metallic electronic structure.[29] However, the metastable nitrogen-rich phases should possess cations in the higher oxidation states, manifesting in useful semiconducting properties, and are thus of particular technological interest for electronic and optoelectronic/photovoltaic applications.

In this study, we employ high-throughput computational screening to explicitly search for metastable nitrogen-rich nitrides. In addition to their potential semiconducting properties, these metastable nitrides are compelling search targets for two reasons: (1) In our recent survey of the thermodynamic metastability of inorganic crystalline solids,[30] we found nitrides to be the chemistry class with the largest fraction of metastable phases, and to have the highest accessible thermodynamic metastability of all inorganic solids, suggesting that crystalline
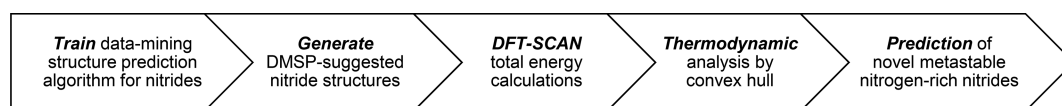
Figure 1. Schematic of the workflow for computational prediction of novel nitrides.

Table 1. Statistics on the Metastability of All Observed and Computable[37] Crystalline Solids in the Inorganic Crystal Structure Database

	nitrides	oxides	all inorganic solids
no. of unique ICSD phases	1253	13 497	29 902
percent metastable ($T = 0$ K)	59.8%	56.0%	51.6%
$\Delta H(E - E_{GS})$ − median	67 meV/atom	15.4 meV/atom	14.9 meV/atom
$\Delta H(E - E_{GS})$ − 90th percentile	190 meV/atom	62 meV/atom	70 meV/atom
median cohesive energy	−6.38 eV/atom	−6.26 eV/atom	−4.88 eV/atom
electronegativity	3.02	3.44	

metastability is readily accessible in the nitrides. (2) We have experimentally demonstrated reactive sputtering with atomic nitrogen precursors as a technique to synthesize highly metastable nitride thin-films.[31,32] These two observations inspire the search for novel metastable nitrides in this relatively uncharted chemical space.

In this work, we begin by briefly reviewing the thermodynamics and bonding of nitrides, with emphasis on the unusual magnitude of their metastability. We then discuss our experimentally validated thermodynamic strategy to synthesize metastable nitrogen-rich nitrides, using reactive nitrogen precursors under constrained equilibrium where the N_2 molecule cannot form. Within this thermodynamic framework, we perform a high-throughput computational search for novel metastable binary nitrides, utilizing a data-mined structure predictor combined with DFT *ab initio* phase stability calculations, following the workflow in Figure 1. Our results demonstrate that even in the relatively simple binary nitride space, there may still be new compounds awaiting experimental discovery.

NITRIDE THERMODYNAMICS

Although the earth's atmosphere is composed of 78% N_2 versus 21% O_2, the majority of observed minerals are oxides, while nitride minerals are considerably more rare. The lack of natural nitrides can largely be attributed to the low chemical reactivity of the N_2 molecule, originating from the extremely stable N_2 triple-bond (bond energy of −9.75 eV). This high N_2 stability also drives correspondingly more-positive nitride formation energies, which, on a per anion basis, is an average of 240 meV/anion more positive than oxide formation energies.[33] For this reason, metals that would nitridize generally oxidize instead, which underlies the rarity of nitride minerals in nature, and also the difficulty of phase-pure nitride synthesis under ambient conditions.

The small formation enthalpies of nitrides might suggest that they are relatively unstable compared to oxides, but we previously found nitrides to actually possess the greatest average cohesive energies of all materials chemistries.[30] These high cohesive energies partially originate from the 3^- valence state of solid-state nitrogen, which leads to a large electrostatic contribution to the ionic component of the lattice cohesive energy. Additionally, nitrogen has a relatively low Pauling electronegativity for an anion, allowing it to form strong covalent bonds with electropositive elements.[34] This mixed ionic/covalent nature results in highly cohesive solids, with a

diversity of structures far greater than that of the more ionic oxides, and includes structural idiosyncrasies like covalent network solids ($Si(CN)_2$), non-close-packed anions ($Sr_3Ge_2N_2$), metal nitride clusters ($Li_{10}N_3Br$), infinite 1-D covalent chains (Ba_2GaGeN), corrugated layered structures ($Na_2K_{13}W_7N_{19}$), and more.[35,36]

In our previous data-mining study on the thermodynamic scale of inorganic crystalline metastability,[30] we identified a strong correlation between the cohesive energy of a chemistry class, and its accessible thermodynamic metastability, defined by the average enthalpy above the ground-state phase(s). We rationalized that a high cohesive energy can enable the persistence of highly metastable structural arrangements. Nitrides, being the most cohesive chemistry, were also found to have the largest fraction of metastable phases, and the highest accessible thermodynamic metastability of all inorganic solids. As summarized in Table 1, while 50% and 90% of all observed and computable[37] metastable inorganic phases are found within 15 and 70 meV/atom of the hull, respectively, for nitrides the median and 90th percentile of metastability are 67 and 190 meV/atom. This metastability threshold is significantly higher than what is typically considered in computational materials searches, and suggests that chemistry-specific tolerances on metastability should be implemented during computational screenings for novel materials.

SYNTHESIS STRATEGY FOR METASTABLE NITROGEN-RICH NITRIDES

A general principle for the synthesis of metastable phases is to identify conditions of "constrained equilibrium", where the formation of the equilibrium phases is kinetically inhibited. In Figure 2, we illustrate a strategy to synthesize metastable nitrides under constrained equilibrium, visualized using the convex hull formalism, which plots nitride formation energies against their compositions. Thermodynamically stable phases lie on the *convex hull*, denoted by the convex curve connecting phases on the lowest-energy envelope. Metastable phases have an energy above the convex hull, and the energy above the hull is a measure of their thermodynamic metastability.

Because the N_2 molecule is so stable, nitrides often possess small or positive formation energies. A rational design route to solid-state nitrides, then, is to synthesize nitrides using nitrogen precursors that are not so strongly bound. Indeed, most successful nitride syntheses exercise this strategy. Examples include ammonolysis, where instead of N_2, ammonia is used as a nitrogen source to convert oxide and halide precursors to
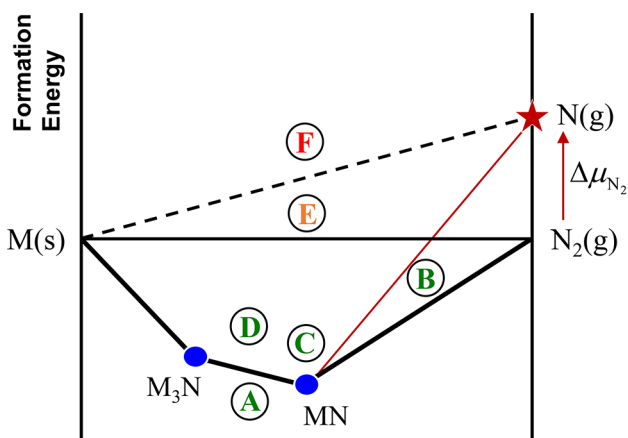
Negative Formation Energy w.r.t Ambient Conditions

A. Stable Compound
B. Stabilizable by Reactive Nitrogen Precursors
C. Metastable Polymorph
D. Metastable Phase-Separating
E. Negative Formation Energy w.r.t Sputtering
F. No Thermodynamic Driving Force

Figure 2. Schematic convex hull in a binary metal−nitrogen space, with an arbitrary metal specified as M. Under constrained equilibrium, where N_2 does not form, and where the nitrogen precursor is available in a more reactive form than N_2, the convex hull should be drawn with respect to the higher chemical potential nitrogen precursor, which could stabilize the metastable phase (B) on the nitrogen-rich portion of the convex hull.

nitrides.[33] Azide precursors can also provide high nitrogen activity for nitride synthesis, as they decompose as $N_3^-(g) \rightarrow N_2 + N + e^-$, yielding a "free" highly reactive nitrogen atom.[38] Nitrogen fugacity under pressures up to 50 GPa was extrapolated from thermochemical data[39] to have a chemical potential up to $+15\ k_BT/N_2$ above the N_2 standard state (∼1.25 eV/N at 2000 K).[40] Another extreme case of reactive nitrogen precursors is atomic nitrogen, which can be made from the cracking of N_2 molecules in the plasma of reactive-sputtering processes. We previously used low-temperature reactive sputtering to synthesize thin-films of metastable Cu_3N and Sn_3N_4 semiconductors,[31,32] and determined from measured phase boundaries that this technique can yield nitrogen chemical potentials up to +1 eV/N above standard-state N_2. A similar plasma-based synthesis was used to synthesize Na_3N, which was also confirmed to be metastable.[41,42] Syntheses of metastable nitrides often require low-temperature reaction conditions, which kinetically inhibit decomposition into gaseous N_2 or transformation to equilibrium phase(s).[43]

Under constrained equilibrium, where reactive nitride precursors cannot recombine to form N_2, phase stability on the nitrogen-rich end should be calculated with respect to the chemical potential of the reactive nitrogen precursor. This may "stabilize" nitrogen-rich metastable nitrides (Figure 2B), as they are above the convex hull with respect to standard-state gaseous N_2, but are below the hull connected with the reactive precursor. The formation energies of many transition metal nitrides are less than −1 eV/atom in magnitude, and because the chemical potential of reactive sputtered monatomic nitrogen can be +1 eV/N, there exists a large thermodynamic window for a metastable nitride to stabilize. The NH_3 precursor

of ammonolysis reactions can also be placed on the nitrogen axis of Figure 2B, by the following half reaction: $\mu_N = \mu_{NH_3} - 3/2\ \mu_{H_2}$, yielding $\Delta\mu_{N_2} = +0.46$ eV/N at standard state. If there is ambient oxygen, the partial pressure of oxygen can also influence $\Delta\mu_{N_2}$, by $\mu_N = \mu_{NH_3} - {}^3/_2\mu_{H_2O} + {}^3/_2\mu_{O}$[44] although oxide products may be thermochemically competitive with desired nitrides.

The use of reactive nitrogen precursors specifically promotes the formation of nitrogen-rich metal nitrides, with cations in the highest possible oxidation states.[29] Syntheses of oxides with reactive oxygen precursors, such as peroxide and ozone, have also resulted in highly oxidized transition metal cations,[45] suggesting that the use of high chemical potential anion precursors may be a general strategy to achieve high metal oxidation states. In summary, the low chemical potential of N_2 drives metal−nitride compositions toward the nitrogen-poor "subnitrides", where the nitrogen atom occupies interstitial sites of a metal sublattice (analogous to metal carbides) and does not adopt an anionic charge, leading to metallic electronic structures. On the other hand, nitrides with the transition metal in higher oxidation states should have N^{3-} anions, resulting in semiconducting properties.

Nitrogen-rich metastable nitrides may also serve as precursors to metastable reduced nitrides, if the nitrogen-rich nitride is reduced under elevated temperatures and reducing agents (such as H_2 gas). Once a reduced nitride has nucleated on a nitrogen-rich nitride, supersaturation under mild conditions could yield further crystal growth on the reduced solid. We previously used this technique to synthesize metastable SnN from metastable Sn_3N_4.[46] The characterized X-ray diffraction pattern for SnN was found to be consistent with not the lowest-energy SnN polymorph, but rather one that was structurally related to Sn_3N_4, suggesting that Sn_3N_4 may have heterogeneously templated the more thermodynamically metastable SnN structure.

In the current investigation, we have focused our predictions on new nitrogen-rich metastable nitrides stabilizable under high nitrogen chemical potential (Figure 2B). Plausibly, any metastable phase with negative formation energy with respect to sputtering conditions (Figure 2, C/D/E) could be kinetically favorable by preferential nucleation on coherent epitaxial substrates.[47,48] However, explicitly identifying these materials and the conditions of their kinetic preference will require more calculations, and are beyond the scope of this study. Readers interested in polymorphs (Figure 2C) and nitrogen-poor compounds that phase separate into other condensed phases (Figure 2D), can access these structures from the Materials Project[49] and the NREL Materials Database for free.[50] Metastable phases with positive formation enthalpy with respect to sputtering conditions (Figure 2F) are not thermodynamically accessible and thus cannot form under these conditions.

■ **METHODS**

Data-Mined Nitride Prediction. To identify novel nitrides, we employ a data-mined structure-prediction algorithm (DMSP),[6,51−53] which makes rational chemical substitutions on existing crystal structures to generate new unobserved phases *in silico*. By computing the formation free-energies of DMSP-suggested phases in DFT, and then comparing the formation energies of these phases against the known convex hull, we can identify novel stable nitrides and stabilizable nitrides. We previously used this technique to identify new stable ternary oxides.[6]

We train the DMSP on the Inorganic Crystal Structure Database (ICSD), mapping isostructural compounds and identifying which cations are statistically prone to substitute for one another. We can train the DMSP on all ICSD compounds, but the ICSD is dominated by oxides, and it is unclear if a substitution matrix trained on oxides also applies to nitrides. On the other hand, training the DMSP on only the sparser nitride space has an order of magnitude fewer data-points than oxides to train on. We test the predictive power of a DMSP trained on four different chemical spaces: (i) nitrides only; (ii) nitrides, phosphides, arsenides, and antimonides (N + P + As + Sb); (iii) nitrides and oxides (N + O); and (iv) nitrides, oxides, phosphides, arsenides, and antimonides (N + O + P + As + Sb). The training is performed on all compounds, not just binaries, and substitutions are designed to allow for ternaries to act as candidates for mixed-valent binary nitrides.

For a given composition, the DMSP provides a list of candidate structures, and the predictive power of a DMSP is evaluated on the basis of its ability to "predict" the structure of a known compound within the list of candidate structures. To compare the predictive power of the four chemical spaces as training sets, we perform 10-fold cross-validation, meaning each data set is parsed into 10 subsets, and then the DMSP is trained on 9 sets and is validated for its ability to recover the structures in the 10th set. This process is repeated 10 times, using each subset as a validation set, and the 9 remaining subsets for training. Figure 3 compares the predictive ability of the DMSP
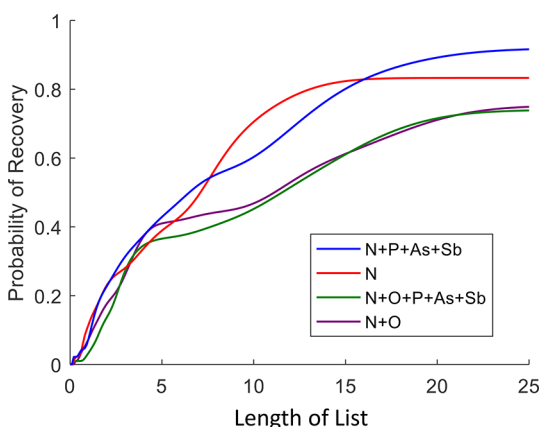
Figure 3. 10-fold cross-validation showing the probability to recover a known nitride from a structural candidate list when the data-mined structure predictor is trained on four different chemical spaces. The number of unique entries in each training space are the following: O, 14622; N, 3105; P, 3422; As, 1357; Sb, 1423. Asymptotes in the probability of recovery are due to unique structural prototypes in the validation data set that are not in the training data set.

trained on the four chemical spaces, where the probability of recovering a structure in the validation set is shown as a function of the length of the candidate structure list. We find the most predictive set to be the set of all pnictides (N + P + As + Sb), which has superior prediction capability to either oxide-containing set, and is better than just nitrides for long prediction lists.

Our cross-validation results show that adding oxides to a DMSP training set is not beneficial for predicting nitrides, indicating that cation chemistry influences oxide and nitride structures differently. Figure 4 shows the data-mined substitution matrix for the 40 most common ionic substitutions in a DMSP, trained for nitrides and trained for oxides, where darker sections indicate higher probability for ionic substitution. We identify from Figure 4 two main differences between cation chemistry in oxides and nitrides. (1) The nitride substitution matrix shows numerous regions of unobserved substitutions, whereas oxides are observed to exhibit greater flexibility in ionic substitution. Both oxides and nitrides prefer homovalent substitutions, although while heterovalent substitutions in the oxides are commonplace, the 2+/3+ substitution is rare in the nitrides, with

exceptions in Mn, Fe, Co, and Cr cations. (2) In general, redox-active metals exhibit lower oxidation states in nitrides than in oxides, for example, TiN vs TiO_2, or MoN vs MoO_3, meaning that common ionic substitutions in high-valence state oxides may not apply to nitride chemistries. These two factors explain why the oxide-trained DMSP is not effective for nitrides, and more generally suggests that DMSP training should be chemistry-specific.

Because predicted structures are constructed by substitution on observed structures, if the structural prototype of a particular nitride has never been observed, the DMSP cannot predict its structure. However, by the variational principle, the true nitride structure will be lower in energy than the DMSP-suggested structure, and so DMSP results are still useful for probing novel low-energy *compositions* within a chemical space. However, because the electronic and optical properties of these nitrides are structure dependent, more sophisticated structure-prediction calculations should be performed in these chemical spaces before assertion of their properties.

Using the substitution matrix, we used the DMSP to suggest 1605 new possible nitride phases for 140 binary M−N compositions, where M includes all alkali metals, alkali earth metals, transition metals, precious metals, and main group elements, up to atomic number 83 (Bi), excluding Be, Tc, Hg, Tl. Formation energies for these suggested phases are then computed in density functional theory, and stability is evaluated in the convex hull formalism described earlier.

Density Functional Theory Calculations. Predicting the critical $\Delta\mu_{N_2}$ that stabilizes a metastable nitrogen-rich nitride relies on accurate formation energies for both the nitrogen-rich phase, and for the next-reduced nitride in composition space. DFT calculations of formation energies typically require correction schemes when one of the elemental end-members is a diatomic molecule at standard state, which is the case for nitrides. We benchmarked two correction schemes for computing nitride formation energies: the fitted elemental reference energies (FERE),[54,55] as used in the NREL Materials Database,[50] and a gas-fit correction scheme,[56] as used in the Materials Project database.[49] Both schemes aim to minimize formation energy errors using a linear least-squares fit on elemental reference energies, but in the FERE scheme, the fit is performed on *all* elemental-phase chemical potentials, whereas in the gas-fit scheme, only the N_2 gas chemical potential is fitted. Both schemes predict formation energies of binary nitrides similarly well, with an RMSE = 0.117 eV/atom for the FERE scheme, and an RMSE = 0.103 eV/atom for the gas-fit correction scheme.

However, we found that the critical $\Delta\mu_{N_2}$ as calculated from the two schemes can differ by up to 2 eV/N under some circumstances, which is a qualitative difference between "synthesizable" and "not synthesizable". In particular, this occurs when competing nitride phases are close in stoichiometry, such that small differences in the predicted formation enthalpy become amplified in $\Delta\mu_{N_2}$. We found the discrepancy between schemes to originate primarily from their different treatments of nitride electronic structures, which can vary from metallic subnitrides to semiconducting nitrogen-rich nitrides. The FERE scheme was originally designed for semiconducting or insulating metal−nonmetal compounds[54,55] and uses GGA+U for transition metal cations. In metallic subnitrides, this approach can lead to unphysical positive formation energies that are inconsistent with experiment. The gas-fit scheme, which uses GGA for all compounds, accurately calculates exothermic formation energies for many observed metallic subnitrides, but likely overstabilizes the semiconducting nitrogen-rich nitrides. A general trend emerges where FERE likely overestimates critical $\Delta\mu_{N_2}$ for metastable nitrogen-rich nitrides, whereas the GGA-based gas-fit scheme likely underestimates the critical $\Delta\mu_{N_2}$. Detailed discussion and analysis of benchmarking results can be found in Supporting Information SI.1.

We ultimately base our thermodynamic analysis on a gas-fit correction scheme, while using the recently released SCAN (strongly constrained and appropriately-normalized) metaGGA functional.[57] The SCAN functional is theoretically superior than PBE-GGA at the calculation of densities and energies in solids with mixed bonding and
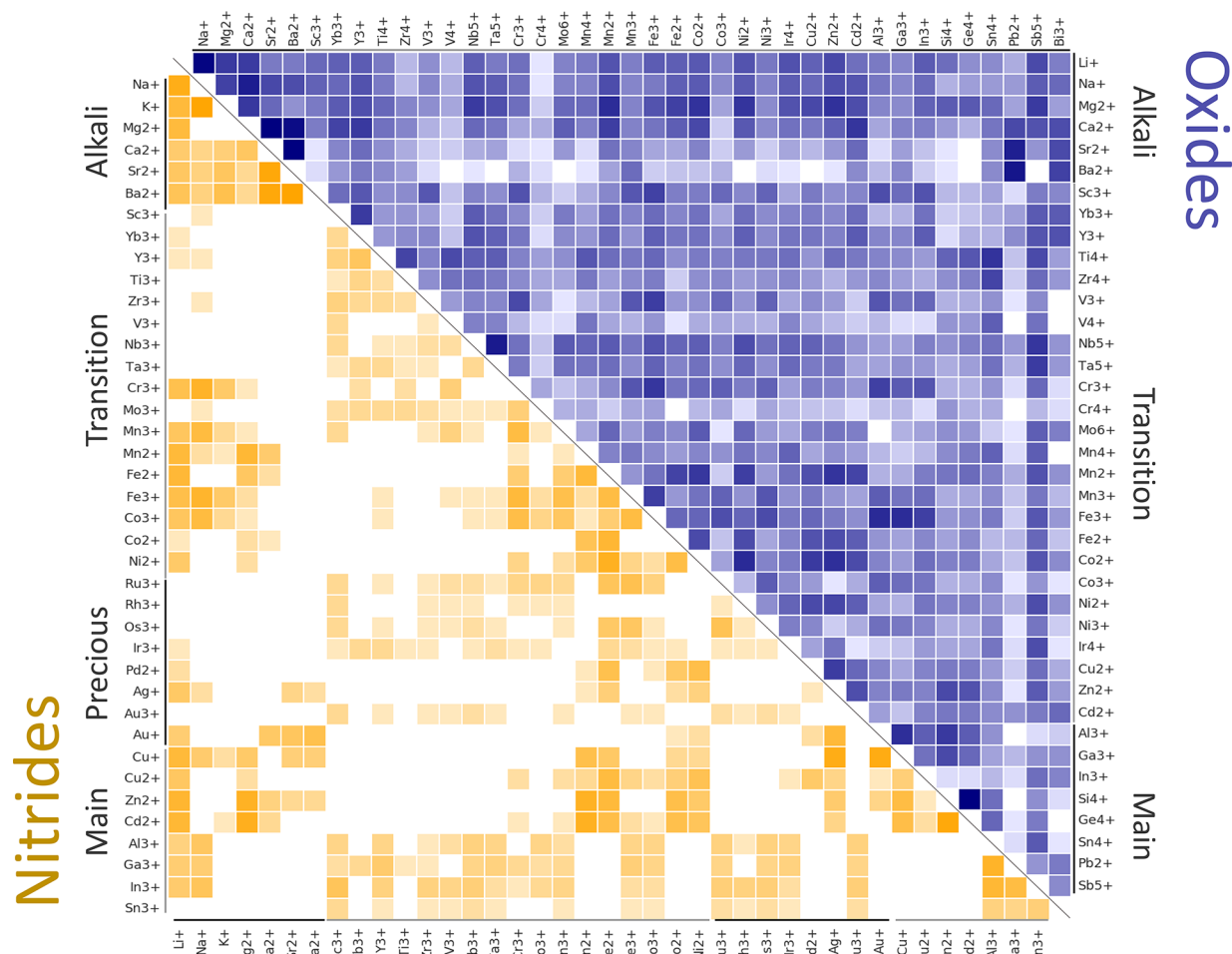
Figure 4. Data-mined substitution matrix for nitrides (orange) trained on the nitrides + pnictides, compared to the substitution matrix for oxides (blue) trained on the oxides. The 40 most common substitutions are shown. Darker tiles correlate to higher probabilities of ionic substitution, with a log probability threshold of −5 for the darkest tiles, and −11 for the lightest tiles, as described in ref 52.

electronic structures,[58] and exhibits more accurate polymorph energy rankings for some transition metal oxides.[59] Figure 5 shows SCAN nitride formation energies benchmarked against known experimental formation energies of binary nitrides, yielding an RMSE = 0.099 eV/
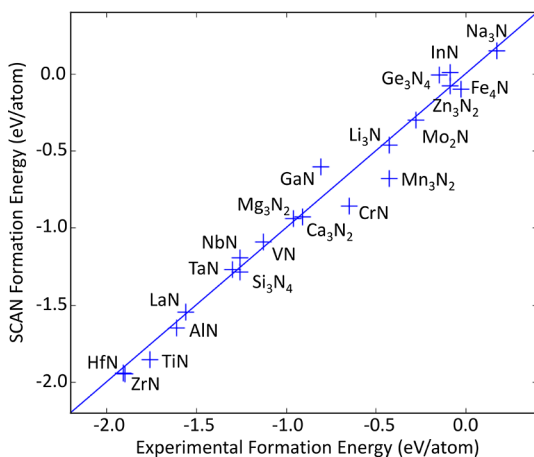
Figure 5. Binary nitride formation energies from DFT-SCAN compared to experiment. The nitrogen reference chemical potential is fitted to −18.79 eV/N$_2$, yielding RMSE = 0.099 eV/atom, compared to the "molecule-in-a-box" chemical potential of −19.17 eV/N$_2$ (with RMSE = 0.128 eV/atom).

atom. By careful investigation of the convex hulls (Figure 6), it appears that SCAN accurately reproduces negative formation energies in the subnitride region, while not overstabilizing the nitrogen-rich phases as from a PBE-GGA scheme. The SCAN critical $\Delta\mu_{N_2}$ is generally found to be in-between the $\Delta\mu_{N_2}$ as calculated from the gas-fit and FERE schemes, and therefore offers a practical compromise between the gas-fit and FERE correction schemes for identifying stabilizable nitrogen-rich nitrides.

Total energies of known and DMSP-suggested nitrides were calculated with density functional theory using the Vienna *ab initio* software package (VASP),[60,61] using the projector augmented-wave method with the SCAN metaGGA functional. Plane-wave basis cutoff energies are set to 520 eV. The k-point densities were distributed within the Brillouin zone in a Monkhorst−Pack grid,[62] or on a Gamma-centered grid for hexagonal cells, and used default k-point densities in compliance with NRELMatDb and Materials Project calculation standards, which were calibrated to achieve total energy convergence of better than 0.5 meV/atom. Each structure is initiated in ferromagnetic, ferrimagnetic, and antiferromagnetic spin configurations, and the lowest-energy configuration is used for phase stability calculations. DFT relaxations that resulted in "phase-separated" unit cells with metal slabs and N$_2$ molecules were removed from the data set. Phase stability calculations are computed using the phase diagram analysis package in Pymatgen,[63] calculated with respect to known nitride phases from the Materials Project,[49] attained using the Materials Project REST API,[64] and with total energies recalculated in SCAN.
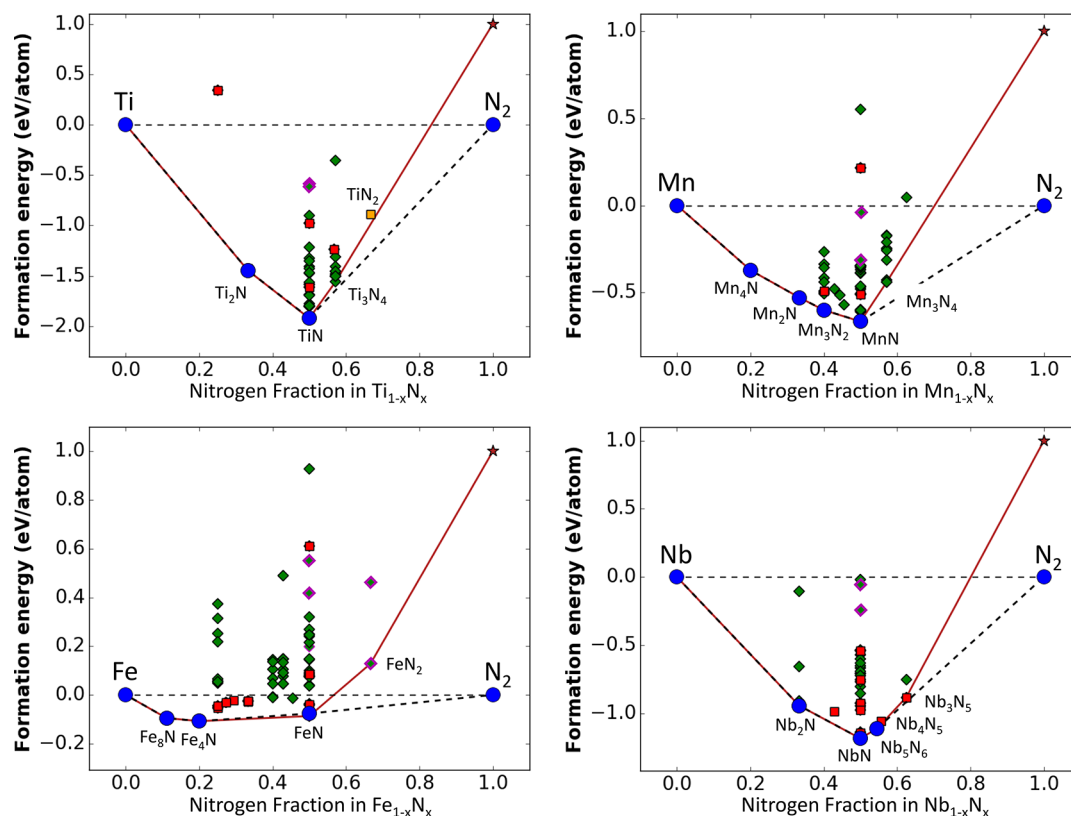
Figure 6. Calculated convex hulls for Ti−N, Mn−N, Fe−N, and Nb−N systems. The convex hull formed by the dashed line is the convex hull under standard-state N_2 gas, and the red convex hull is with respect to a nitrogen chemical potential of +1 eV/N. Blue circles indicate known ground-states in the ICSD that are stable phases on the convex hull. Red squares are known metastable ICSD phases, and green diamonds are DMSP-predicted phases from this work. Materials with magenta borders have N−N bond lengths comparable to pernitrides.

■ RESULTS AND DISCUSSION

From the DFT calculated phase stability of the 1605 binary nitrides suggested by the data-mined structure predictor, we found 22 to be stabilizable under $\Delta\mu_{N_2}$ = +1 eV/N, and 9 more to be stabilizable by $\Delta\mu_{N_2}$ = +1.5 eV/N. Nitrides that are metastable but stabilizable under high nitrogen chemical potential were found in binary nitride systems with the following cations: Bi, Cr, Cu, Fe, Ir, Mn, Mo, Os, Pb, Pd, Pt, Re, Ru, Sb, Sn, Ti, and V. These binary nitride systems tend to have either shallow convex hulls (formation energy of the "deepest" phase less negative than −0.5 eV/atom), or no known stable phases. Our calculated stabilizable binary nitrides are exhibited in Table 2, along with their ICSD or DMSP provenance and thermodynamic (meta)stability properties. For a detailed investigation, readers are invited to view the convex hulls for the aforementioned stabilizable systems in Supporting Information SI1.3.

Metastable Nitrides That Can Be Stabilized by Reactive Nitrogen Precursors. Because the N_2 molecule has such low chemical potential, convex hulls in transition metal nitrides tend to be pinned at low nitrogen compositions, such that the stable nitrides typically have metal cations in a reduced oxidation state. However, by increasing the nitrogen chemical potential, we predict a host of stabilizable high oxidation-state nitrides for the transition metal systems V−N, Mn−N, Cr−N, Mo−N, and Nb−N, many of which have not yet been reported or hypothesized in the literature.

We predict that the transition metal nitrides V_3N_4, Cr_3N_4, and Mn_3N_4 can be stabilizable under nitrogen chemical

potentials of +0.30, +0.92, and +0.92 eV/N, respectively. The critical $\Delta\mu_{\text{to be stabilized under a very high} N_2}$ for V_3N_4 is calculated with respect to the rock-salt VN, which is the stable phase under ambient conditions. The 4+ oxidation state is common in the oxides of vanadium, chromium, and manganese, and so it is not surprising that it is found in nitride systems, under suitably high nitrogen chemical potential. None of these phases have previously been reported in the literature, in either experimental or theoretical studies. We also predict a new phase Nb_3N_5, isostructural to the Ta_3N_5 structure, that is stabilizable under a relatively mild +0.20 eV/N. Nb_3N_5 has not been reported in the scientific literature, although a recent patent reports its synthesis,[65] and measures a band gap of 1.6 eV, suggesting it may be a promising semiconductor for solar energy conversion applications.

Titanium nitride, Ti_3N_4, has been extensively sought after,[66] as Hf_3N_4, Zr_3N_4, Si_3N_4, and Ge_3N_4 are all known to exist, but Ti_3N_4 does not. Its properties have been the subject of numerous computational studies,[67,68] but its experimental synthesis has not been conclusively established.[69] We calculate that although Ti_3N_4 is only 90 meV/atom above the hull, which is within the thermodynamic range of observed metastable nitrides, due to its compositional proximity to the very stable TiN, it can only be stabilized under N_2 chemical potentials of +0.60 eV/N. Although this may be accessible under reactive sputtering, this is likely above the chemical potential range of ammonolysis, which was the primary synthesis methodology in the past. We also computed a recently synthesized titanium pernitride, TiN_2, to be stabilized under a very high $\Delta\mu_{N_2}$ =

Table 2. Metastable Nitrogen-Rich Nitrides Stabilizable by Reactive Nitrogen Precursors[a]

nitride compd	prototype ICSD ID	prototype structure	space group	E abv hull (eV/atom)	decomp products	pernitride	critical μN_2 (eV/atom)
RuN_2*[b]	167872	RhN_2	$F\bar{4}3m$	0.10	$Ru + N_2$	N	0.20
Nb_3N_5	76460	Ta_3N_5	$Cmcm$	0.03	$Nb_5N_6 + N_2$	N	0.20
Sn_3N_4*[c]	89525	Sn_3N_4	$Fd\bar{3}m$	0.16	$Sn + N_2$	N	0.29
V_3N_4	100135	Si_3N_4	$P2_1/m$	0.04	$VN + N_2$	N	0.30
ReN_2*[d]	187441	ReN_2	$C2/m$	0.23	$Re_3N + N_2$	Y	0.41
RuN_2*[b]	240754	RuN_2	$Pmnn$	0.30	$Ru + N_2$	N	0.45
PtN_2*[e]	166462	PtN_2	$Pa\bar{3}$	0.30	$Pt + N_2$	Y	0.45
ReN	162871	BN	Cm	0.16	$Re_3N + N_2$	N	0.48
OsN_2*[f]	260545	OsN_2	$P6/mmm$	0.35	$Os + N_2$	N	0.52
FeN_2	240759	OsN_2	$Pnnm$	0.18	$FeN + N_2$	Y	0.54
IrN_2*[f]	240755	IrN_2	$P2_1/c$	0.38	$Ir + N_2$	Y	0.57
Ti_3N_4	78944	Zr_3N_4	$Pnma$	0.09	$TiN + N_2$	N	0.60
Re_3N_4	156339	Ge_3N_4	$Pnma$	0.27	$Re_3N + N_2$	N	0.64
PdN_2*[g]	191244	PdN_2	$Pnnm$	0.44	$Pd + N_2$	Y	0.65
Re_3N_5	95782	P_3N_5	$Imm2$	0.34	$Re_3N + N_2$	N	0.68
Re_2N	181874	Re_2N	$P6_3/mmc$	0.08	$Re_3N + N_2$	N	0.72
SbN	162883	BN	P_21/c	0.40	$Sb + N_2$	N	0.80
Cu_2N_2	60168	MoN	$P\bar{1}$	0.40	$Cu + N_2$	Y	0.81
CrN_2	240754	RuN_2	$Pnnm$	0.27	$CrN + N_2$	Y	0.82
Na_3N*[h]	421115	Na_3N	$Pm\bar{3}m$	0.21	$Na + N_2$	N	0.84
Cr_3N_4	156339	Ge_3N_4	$Pnma$	0.13	$CrN + N_2$	N	0.92
Mn_3N_4	100135	Si_3N_4	$P2_1/m$	0.13	$MnN + N_2$	N	0.92
Mo_3N_5	95782	P_3N_5	$Imm2$	0.22	$MoN + N_2$	N	0.97
Ti_3N_4	92156	Si_3N_4	$P31c$	0.14	$TiN + N_2$	N	1.00
Cu_3N*[I]	53313	Cu_3N	$Pm\bar{3}m$	0.26	$Cu + N_2$	N	1.04
Pb_3N_2	91273	$NiSr_2N_2$	$Pnma$	0.42	$Pb + N_2$	N	1.05
TiN_2*[j]	N/A	TiN_2	$I4/mcm$	0.39	$TiN + N_2$	N	1.18
MoN_2*[l]	260549	OsN_2	$P4/mbm$	0.38	$MoN + N_2$	Y	1.23
Pb_3N_4	41952	C_3N_4	$R3m$	0.75	$Pb + N_2$	Y	1.32
Pb_3N_2	182699	Nb_2N_3	$Pnma$	0.54	$Pb + N_2$	N	1.35
Mo_2N_3	16528	$MoNCl_3$	$P\bar{1}$	0.24	$MoN + N_2$	N	1.37
BiN	162876	BN	$Pnma$	0.72	$Bi + N_2$	N	1.44
Pd_3N_2	162795	Ca_3N_2	$C2/m$	0.58	$Pd + N_2$	N	1.46

[a]Prototype structure refers to the compound from which the structure originated. A prototype structure which is the same as the compound in column 1 indicates that the compound was previously known. If not, then the structure is predicted by DMSP. If the prototype structure of the true nitride has not been observed previously, experiment may find a lower-energy structure for these compositions. Starred nitrides indicate previously synthesized compounds. TiN$_2$ was synthesized in 2016 and did not have an ICSD entry at the time of this publication. [b]Ref 87. [c]Ref 31. [d]Ref 74. [e]Ref 84. [f]Ref 88. [g]Ref 85. [h]Ref 41. [I]Ref 32. [j]Ref 70. [l]Ref 79.

+1.18 eV/N,[70] suggesting that perhaps with careful annealing under lower pressure Ti$_3$N$_4$ may be isolated.

Since the synthesis of Re$_3$N in 2010,[71] many experimental and computational studies have targeted the higher-nitrogen rhenium nitrides.[72] We predict a broad collection of nitrogen-rich rhenium nitrides with compositions ReN, Re$_3$N$_4$, Re$_3$N$_5$, and ReN$_2$ that are all within 350 meV/atom above the hull and can be stabilized under $\Delta\mu_{N_2}$ up to +0.5 eV/N. ReN$_2$ may have been synthesized in 2012,[73] and was claimed to have the MoS$_2$ crystal structure, although this has been contested in a computational study.[74] Our predictions of intermediate ReN (+0.48 eV/N), Re$_3$N$_4$ (+0.64 eV/N) and Re$_3$N$_5$ (+0.68 eV/N) compositions are in a thermodynamic range that suggests that careful tuning of the experimental $\Delta\mu_{N_2}$ during synthesis may yield a variety of novel rhenium nitrides.

Of the main group nitrides, we identify a new metastable antimony nitride, SbN, that is 400 meV/atom above the hull with respect to standard-state N$_2$, but can be stabilized under $\Delta\mu_{N_2}$ = +0.8 eV/N. Crystalline antimony nitrides have never been reported before, although SbN has been reported in molecular form,[75] and Sb$_3$N was previously made in amorphous

form.[76] The computed thermodynamic conditions for the synthesis of SbN are less aggressive than for Cu$_3$N, which was synthesized under reactive-sputtering conditions, which suggests that synthesis of this compound may be promising.

Finally, we also predict post-transition metal nitrides BiN, Pb$_3$N$_2$, and Pb$_3$N$_4$, that may be stabilizable under very high nitrogen chemical potentials. BiN was previously synthesized as a nitridizing agent,[77] although its crystal structure was not determined, as it was noted that it was highly metastable and would explode upon mechanical shock. We calculate BiN to be 720 meV/atom above the hull, and stabilizable only under +1.44 eV/N, so it is remarkable that solid BiN could be prepared. We also predict a Pb$_3$N$_4$, at 750 meV/atom above the hull, and Pb$_3$N$_2$, at 420 meV/atom above the hull, which may be stabilized with +1.32 and +1.05 eV/N, respectively. Although these lead nitrides might be synthesizable, they may decompose explosively like BiN, as heavy main group cations tend not to contribute significantly to the lattice cohesive energy, suggesting low kinetic barriers for N$_2$ decomposition. Although not as metastable as the Bi- and Pb-nitrides, we have previously found bulk powders of Cu$_3$N to explode above 70

°C, but found our Cu_3N thin-films to be shelf-stable for over a year, suggesting that thin-films of metastable solids may exhibit enhanced resistance to decomposition.

In 2015, a novel molybdenum nitride with composition MoN_2 was reported, synthesized under mild pressures, and found to crystallize in the rhombohedral MoS_2 structure with $R3m$ symmetry.[78] When we calculate the MoN_2 phase in this MoS_2 structure, we found it to be 690 meV/atom above the hull, and that it could not be stabilized under reasonable nitrogen chemical potentials, due to its compositional proximity to the very stable MoN phase. In agreement with a recent computational structure prediction study, we also calculated a pernitride in the $P4/mbm$ symmetry to be the lowest-energy structure, stabilizable under 1.23 eV/N.[79] It will be interesting to determine the mechanisms that yield the formation of MoN_2 in the $R3m$-MoS_2 structure, and to understand the factors that give preference to this structure over the lower-energy MoN_2 structures. We also predicted Mo_3N_5 and Mo_2N_3 phases in the Mo−N system, with critical $\Delta\mu_{N_2}$ of +0.97 and +1.37 eV/N, respectively.

Pernitrides. Pernitrides are a prominent class of metastable, nitrogen-rich binary nitrides that consist of an N_2^{4-} anion of bond order 1 (isoelectronic to an F−F bond). The metastable pernitrides are in contrast to the stable alkali earth diazenides, CaN_2, SrN_2, and BaN_2, of bond order 2 (isoelectronic to O=O) which can be synthesized by decomposition of the corresponding azides under high pressure.[80] The discovery of PtN_2 and IrN_2 under high-pressure synthesis,[81−84] coupled with their high bulk moduli (~400 GPa), spurred an extensive effort to synthesize such ultraincompressible materials. In the past decade, all of the precious metal pernitrides have been synthesized, spanning IrN_2, PtN_2, PdN_2, RuN_2, RhN_2, and OsN_2.[85−88] These precious metal pernitrides exist primarily in the pyrite or marcasite structure, and are metastable under ambient conditions. We calculate their standard-state formation enthalpies to be in the range +200 to +450 meV/atom, requiring $\Delta\mu_{N_2}$ up to about +0.7 eV/N.

Very recently, titanium pernitride, TiN_2, was investigated theoretically,[89,90] and was then synthesized under high-pressure synthesis at 73 GPa, with a bulk modulus in the range 360−385 GPa.[70] We calculate the $\Delta\mu_{N_2}$ for TiN_2 to be +1.18 eV/N, much higher than the precious metal pernitrides. The existence of TiN_2 suggests that other transition metal pernitrides may be synthesizable. In this work, the DMSP algorithm also predicts the existence of an iron pernitride, FeN_2, under $\Delta\mu_{N_2}$ = +0.54 eV/N, and a chromium pernitride, CrN_2, under $\Delta\mu_{N_2}$ = +0.82 eV/N. While FeN_2 was recently proposed from a theoretical study and found to be stabilizable under 17 GPa,[91] CrN_2 has not yet been discussed in the literature. These thermodynamic windows are less aggressive than those for TiN_2 and the other pernitrides, suggesting that they are compelling pernitride targets for experimentalists to investigate via high-pressure synthesis. We also identify a copper(I) pernitride, with composition Cu_2N_2, which may be synthesizable under $\Delta\mu_{N_2}$ = +0.82 eV/N. This is lower than the $\Delta\mu_{N_2}$ = +1.04 eV/N we used to synthesize Cu_3N under reactive sputtering.

Although many of these observed and predicted pernitrides should be thermodynamically accessible under reactive-sputtering nitrogen chemical potentials of +1 eV/atom, pernitride synthesis has universally involved high-pressure reactions, and pernitrides have never been observed via solid-state ammonolysis, or reactive-sputtering methods. This opens up the question of whether or not there is a special pressure-activated component of high-pressure synthesis required to yield pernitrides. Indeed, transition metal nitrides (e.g., TiN, MoN, RuN, CrN) are routinely deposited by sputtering, yet their corresponding pernitrides have never been reported in thin-film form. Elucidating the intermediate steps in the formation pathway of pernitride anions will determine if pressure is a necessary component of pernitride synthesis, and if not, if there are industrial-compatible synthesis techniques, such as sputtering or solid-state synthesis, that could enable their application on a large scale.

We note that the DFT-calculated formation energies of diazenides tend to be more stable in GGA than in SCAN, as can be seen in the Ca−N, Sr−N, and Ba−N hulls in Supporting Information SI.3. We previously found DFT to overstabilize peroxides relative to oxides,[92] and hypothesize that such overstabilization may also be occurring for diazenides and pernitrides in unmodified GGA.

■ CONCLUSIONS

Our recent identification of the extraordinary metastability of solid-state nitrides, coupled with rational experimental strategies to synthesize them, inspired this targeted computational search for novel metastable nitrogen-rich nitrides. Our data-mined ionic substitution structure predictor identified novel metastable nitrogen-rich binary nitrides in transition metal and main group nitride systems, that were then calculated by DFT to be stabilizable under reactive nitrogen precursors. Notably, we predicted the nitrogen-rich transition metal binary nitrides Mn_3N_4, Cr_3N_4, V_3N_4, and Nb_3N_5, and the main group nitride SbN, which should all be stabilizable under reactive sputtering with low temperature, and low target−substrate distances, which can achieve $\Delta\mu_{N_2}$ = +1 eV/N. We also predicted the pernitrides FeN_2, CrN_2, and Cu_2N_2, which have stability windows commensurate with other pernitrides that were successfully synthesized under high-pressure synthesis.

The search strategies we used in this work for binary nitrides can be extendable to ternary and quaternary nitride spaces, including metal−metal nitrides, and metal−anion nitrides such as oxynitrides and fluoronitrides. The enormous combinatorics of the ternary and quaternary spaces have even more possibility for the discovery of novel materials in this underexplored nitride space. More generally, this paper represents a new strategy in high-throughput computational materials design to target metastable materials. By identifying conditions of constrained equilibrium where the formation of ground-state phases is kinetically limited, we devise rational design strategies toward the directed synthesis of metastable compounds. This work can serve as a case study: As experimentalists identify new synthetic routes to exotic or novel materials, these synthesis conditions can be included in thermodynamic screening criteria, to broaden the search space of computational materials design beyond equilibrium phases and compositions.

■ ASSOCIATED CONTENT

Ⓢ Supporting Information

The Supporting Information is available free of charge on the ACS Publications website at DOI: 10.1021/acs.chemmater.7b02399.

Formation energy calibration within two formation energy correction schemes (Gas-fit/FERE); nitride

formation energies using SCAN + gas-fit correction; prediction of new nitride polymorphs in SCAN; and convex hulls in the Gas-fit/FERE/SCAN schemes for Bi, Cr, Cu, Fe, Hf, Ir, Mn, Mo, Nb, Pb, Pd, Pt, Re, Ru, Sb, Sn, Ta, Ti, V, W, and Zr (PDF)

■ AUTHOR INFORMATION

Corresponding Author

*E-mail: gceder@berkeley.edu.

ORCID 📙

Wenhao Sun: 0000-0002-8416-455X

Andriy Zakutayev: 0000-0002-3054-5525

Notes

The authors declare no competing financial interest.

■ REFERENCES

(1) Jain, A.; Shin, Y.; Persson, K. A. Computational predictions of energy materials using density functional theory. *Nat. Rev. Mater.* **2016**, *1*, 15004.

(2) Curtarolo, S.; Hart, G. L. W.; Nardelli, M. B.; Mingo, N.; Sanvito, S.; Levy, O. The high-throughput highway to computational materials design. *Nat. Mater.* **2013**, *12*, 191−201.

(3) Zakutayev, A.; Zhang, X.; Nagaraja, A.; Yu, L.; Lany, S.; Mason, O.; Ginley, D.; Zunger, A. Theoretical prediction and experimental realization of new stable inorganic materials using the inverse design approach. *J. Am. Chem. Soc.* **2013**, *135*, 10048−10054.

(4) Potyrailo, R.; Rajan, K.; Stoewe, K.; Takeuchi, I.; Chisholm, B.; Lam, H. Combinatorial and high-throughput screening of materials libraries: Review of state of the art. *ACS Comb. Sci.* **2011**, *13*, 579−633.

(5) Kirklin, S.; Saal, J. E.; Meredig, B.; Thompson, A.; Doak, J. W.; Aykol, M.; Rühl, S.; Wolverton, C. The Open Quantum Materials Database (OQMD): assessing the accuracy of DFT formation energies. *npj Comput.Mater.* **2015**, *1*, 15010.

(6) Hautier, Geoffroy; et al. Finding nature's missing ternary oxide compounds using machine learning and density functional theory. *Chem. Mater.* **2010**, *22*, 3762−3767.

(7) Ceder, G.; Persson, K. The stuff of dreams. *Sci. Am.* **2013**, *309*, 36−40.

(8) Teter, D. M. Computational alchemy: the search for new superhard materials. *MRS Bull.* **1998**, *23*, 22−27.

(9) Hinuma, Y.; Hatakeyama, T.; Kumagai, Y.; Burton, L. A.; Sato, H.; Muraba, Y.; Iimura, S.; Hiramatsu, H.; Tanaka, I.; Hosono, H.; Oba, F. Discovery of earth-abundant nitride semiconductors by computational screening and high-pressure synthesis. *Nat. Commun.* **2016**, *7*, 11962.

(10) Ching, W. Y.; Mo, S. D.; Ouyang, L.; Rulis, P.; Tanaka, I.; Yoshiya, M. Theoretical prediction of the structure and properties of cubic spinel nitrides. *J. Am. Ceram. Soc.* **2002**, *85*, 75−80.

(11) Sarmiento-Pérez, R.; Cerqueira, T. F.; Körbel, S.; Botti, S.; Marques, M. A. Prediction of stable nitride perovskites. *Chem. Mater.* **2015**, *27*, 5957−5963.

(12) Wittmer, M. Properties and microelectronic applications of thin films of refractory metal nitrides. *J. Vac. Sci. Technol., A* **1985**, *3*, 1797−1803.

(13) Long, G.; Foster, L. M. Aluminum Nitride, a Refractory for Aluminum to 2000° C. *J. Am. Ceram. Soc.* **1959**, *42*, 53−59.

(14) Yamanaka, S.; Hotehama, K.; Kawaji, H. Superconductivity at 25.5 K in electron-doped layered hafnium nitride. *Nature* **1998**, *392*, 580−582.

(15) Chen, X. J.; Struzhkin, V. V.; Wu, Z.; Somayazulu, M.; Qian, J.; Kung, S.; Christensen, A. N.; Zhao, Y.; Cohen, R. E.; Mao, H. K.; Hemley, R. J. Hard superconducting nitrides. *Proc. Natl. Acad. Sci. U. S. A.* **2005**, *102*, 3198−3201.

(16) Waltereit, P.; Brandt, O.; Trampert, A.; Grahn, H. T.; Menniger, J.; Ramsteiner, M.; Reiche, M.; Ploog, K. H. Nitride semiconductors free of electrostatic fields for efficient white light-emitting diodes. *Nature* **2000**, *406*, 865−868.

(17) Ponce, F. A.; Bour, D. P. Nitride-based semiconductors for blue and green light-emitting devices. *Nature* **1997**, *386*, 351.

(18) Zakutayev, A. Design of nitride semiconductors for solar energy conversion. *J. Mater. Chem. A* **2016**, *4*, 6742−6754.

(19) Lu, N.; Ferguson, I. III-nitrides for energy production: photovoltaic and thermoelectric applications. *Semicond. Sci. Technol.* **2013**, *28*, 074023.

(20) Wu, Y.; Lazic, P.; Hautier, G.; Persson, K.; Ceder, G. First principles high throughput screening of oxynitrides for water-splitting photocatalysts. *Energy Environ. Sci.* **2013**, *6*, 157−168.

(21) Yuliati, L.; Yang, J. H.; Wang, X.; Maeda, K.; Takata, T.; Antonietti, M.; Domen, K. Highly active tantalum (v) nitride nanoparticles prepared from a mesoporous carbon nitride template for photocatalytic hydrogen evolution under visible light irradiation. *J. Mater. Chem.* **2010**, *20*, 4295−4298.

(22) Ohkubo, I.; Mori, T. Two-Dimensional Layered Complex Nitrides as a New Class of Thermoelectric Materials. *Chem. Mater.* **2014**, *26*, 2532−2536.

(23) Quintela, C. X.; Rivadulla, F.; Rivas, J. Thermoelectric properties of stoichiometric and hole-doped CrN. *Appl. Phys. Lett.* **2009**, *94*, 152103.

(24) Bernardini, F.; Fiorentini, V.; Vanderbilt, D. Spontaneous polarization and piezoelectric constants of III-V nitrides. *Phys. Rev. B: Condens. Matter Mater. Phys.* **1997**, *56*, R10024.

(25) Tholander, C.; Andersson, C. B. A.; Armiento, R.; Tasnadi, F.; Alling, B. Strong piezoelectric response in stable $TiZnN_2$, $ZrZnN_2$, and $HfZnN_2$ found by ab initio high-throughput approach. *J. Appl. Phys.* **2016**, *120*, 225102.

(26) Sugita, Y.; Mitsuoka, K.; Komuro, M.; Hoshiya, H.; Kozono, Y.; Hanazono, M. Giant magnetic moment and other magnetic properties of epitaxially grown $Fe_{16}N_2$ single-crystal films. *J. Appl. Phys.* **1991**, *70*, 5977−5982.

(27) Stein, A.; Keller, S. W.; Mallouk, T. E. Turning down the heat: design and mechanism in solid-state synthesis. *Science* **1993**, *259*, 1558−1565.

(28) Gopalakrishnan, J. Chimie douce approaches to the synthesis of metastable oxide materials. *Chem. Mater.* **1995**, *7*, 1265−1275.

(29) Salamat, A.; Hector, A. L.; Kroll, P.; McMillan, P. F. Nitrogen-rich transition metal nitrides. *Coord. Chem. Rev.* **2013**, *257*, 2063−2072.

(30) Sun, W.; Dacek, S. T.; Ong, S. P.; Hautier, G.; Jain, A.; Richards, W. D.; Gamst, A. C.; Persson, K. A.; Ceder, G. The thermodynamic scale of inorganic crystalline metastability. *Sci. Adv.* **2016**, *2*, e1600225.

(31) Caskey, C. M.; Seabold, J. A.; Stevanović, V.; Ma, M.; Smith, W. A.; Ginley, D. S.; Neale, N. R.; Richards, R. M.; Lany, S.; Zakutayev, A.

Semiconducting properties of spinel tin nitride and other IV 3 N 4 polymorphs. *J. Mater. Chem. C* **2015**, *3*, 1389−1396.

(32) Caskey, C. M.; Richards, R. M.; Ginley, D. S.; Zakutayev, A. Thin film synthesis and properties of copper nitride, a metastable semiconductor. *Mater. Horiz.* **2014**, *1*, 424−430.

(33) Elder, S. H.; DiSalvo, F. J.; Topor, L.; Navrotsky, A. Thermodynamics of ternary nitride formation by ammonolysis: application to lithium molybdenum nitride (LiMoN2), sodium tungsten nitride (Na3WN3), and sodium tungsten oxide nitride (Na3WO3N). *Chem. Mater.* **1993**, *5*, 1545−1553.

(34) Pauling, L.; Huggins, M. L. Covalent radii of atoms and interatomic distances in crystals containing electron-pair bonds. *Z. Kristallogr. - Cryst. Mater.* **1934**, *87*, 205−238.

(35) Niewa, R.; DiSalvo, F. J. Recent developments in nitride chemistry. *Chem. Mater.* **1998**, *10*, 2733−2752.

(36) Gregory, D. H. Structural families in nitride chemistry. *J. Chem. Soc., Dalton Trans.* **1999**, *3*, 259−270.

(37) See ref 30, Supporting Information, for the criteria for "observed and computable" inorganic solids.

(38) Choi, J.; Gillan, E. G. Solvothermal metal azide decomposition routes to nanocrystalline metastable nickel, iron, and manganese nitrides. *Inorg. Chem.* **2009**, *48*, 4470−4477.

(39) Jacobsen, R. T.; Stewart, R. B.; Jahangiri, M. *J. Phys. Chem. Ref. Data* **1986**, *15*, 735−909.

(40) Kroll, P.; Schröter, T.; Peters, M. Prediction of novel phases of tantalum (V) nitride and tungsten (VI) nitride that can be synthesized under high pressure and high temperature. *Angew. Chem., Int. Ed.* **2005**, *44*, 4249−4254.

(41) Fischer, D.; Jansen, M. Synthesis and structure of Na3N. *Angew. Chem., Int. Ed.* **2002**, *41*, 1755−1756.

(42) Vajenine, G. V. Plasma-assisted synthesis and properties of Na3N. *Inorg. Chem.* **2007**, *46*, 5146−5148.

(43) Sun, W.; Ceder, G. Induction time of a polymorphic transformation. *CrystEngComm* **2017**, *19*, 4576−4585.

(44) Katsura, M. Thermodynamics of nitride and hydride formation by the reaction of metals with flowing NH3. *J. Alloys Compd.* **1992**, *182*, 91−102.

(45) Hiley, C. I.; Lees, M. R.; Fisher, J. M.; Thompsett, D.; Agrestini, S.; Smith, R. I.; Walton, R. I. Ruthenium (V) Oxides from Low-Temperature Hydrothermal Synthesis. *Angew. Chem., Int. Ed.* **2014**, *53*, 4423−4427.

(46) Caskey, C. M.; Holder, A.; Shulda, S.; Christensen, S. T.; Diercks, D.; Schwartz, C. P.; Biagioni, D.; Nordlund, D.; Kukliansky, A.; Natan, A.; Prendergast, D.; et al. Synthesis of a mixed-valent tin nitride and considerations of its possible crystal structures. *J. Chem. Phys.* **2016**, *144*, 144201.

(47) Sun, W.; Jayaraman, S.; Chen, W.; Persson, K. A.; Ceder, G. Nucleation of metastable aragonite CaCO3 in seawater. *Proc. Natl. Acad. Sci. U. S. A.* **2015**, *112*, 3199−3204.

(48) Ding, H.; Dwaraknath, S. S.; Garten, L.; Ndione, P.; Ginley, D.; Persson, K.A. Computational Approach for Epitaxial Polymorph Stabilization through Substrate Selection. *ACS Appl. Mater. Interfaces* **2016**, *8*, 13086−13093.

(49) Jain, A.; Ong, S. P.; Hautier, G.; Chen, W.; Richards, W. D.; Dacek, S.; Cholia, S.; Gunter, D.; Skinner, D.; Ceder, G.; Persson, K. A. Commentary: The Materials Project: A materials genome approach to accelerating materials innovation. *APL Mater.* **2013**, *1*, 011002.

(50) *NREL Materials Database*; materials.nrel.gov, 2016.

(51) Fischer, C. C.; Tibbetts, K. J.; Morgan, D.; Ceder, G. Predicting crystal structure by merging data mining with quantum mechanics. *Nat. Mater.* **2006**, *5*, 641−646.

(52) Hautier, G.; Fischer, C.; Ehrlacher, V.; Jain, A.; Ceder, G. Data mined ionic substitutions for the discovery of new compounds. *Inorg. Chem.* **2011**, *50*, 656−663.

(53) Yang, L.; Ceder, G. Data-mined similarity function between material compositions. *Phys. Rev. B: Condens. Matter Mater. Phys.* **2013**, *88*, 224107.

(54) Stevanović, V.; Lany, S.; Zhang, X.; Zunger, A. Correcting density functional theory for accurate predictions of compound enthalpies of formation: Fitted elemental-phase reference energies. *Phys. Rev. B: Condens. Matter Mater. Phys.* **2012**, *85*, 115104.

(55) Lany, S. Semiconductor thermochemistry in density functional calculations. *Phys. Rev. B: Condens. Matter Mater. Phys.* **2008**, *78*, 245207.

(56) Wang, L.; Maxisch, T.; Ceder, G. A first-principles approach to studying the thermal stability of oxide cathode materials. *Chem. Mater.* **2007**, *19*, 543−552.

(57) Sun, J.; Ruzsinszky, A.; Perdew, J. P. Strongly constrained and appropriately normed semilocal density functional. *Phys. Rev. Lett.* **2015**, *115*, 036402.

(58) Sun, J.; Remsing, R. C.; Zhang, Y.; Sun, Z.; Ruzsinszky, A.; Peng, H.; Yang, Z.; Paul, A.; Waghmare, U.; Wu, X.; Klein, M. L.; Perdew, J. P. Accurate first-principles structures and energies of diversely bonded systems from an efficient density functional. *Nat. Chem.* **2016**, *8*, 831−836.

(59) Kitchaev, D. A.; Peng, H.; Liu, Y.; Sun, J.; Perdew, J. P.; Ceder, G. Energetics of MnO 2 polymorphs in density functional theory. *Phys. Rev. B: Condens. Matter Mater. Phys.* **2016**, *93*, 045132.

(60) Kresse, G.; Furthmüller, J. Efficient iterative schemes for ab initio total-energy calculations using a plane-wave basis set. *Phys. Rev. B: Condens. Matter Mater. Phys.* **1996**, *54*, 11169.

(61) Kresse, G.; Furthmüller, J. Efficiency of ab-initio total energy calculations for metals and semiconductors using a plane-wave basis set. *Comput. Mater. Sci.* **1996**, *6*, 15−50.

(62) Monkhorst, H. J.; Pack, J. D. Special points for Brillouin-zone integrations. *Phys. Rev. B* **1976**, *13*, 5188.

(63) Ong, S. P.; Richards, W. D.; Jain, A.; Hautier, G.; Kocher, M.; Cholia, S.; Gunter, D.; Chevrier, V. L.; Persson, K. A.; Ceder, G. Python Materials Genomics (pymatgen): A robust, open-source python library for materials analysis. *Comput. Mater. Sci.* **2013**, *68*, 314−319.

(64) Ong, S. P.; Cholia, S.; Jain, A.; Brafman, M.; Gunter, D.; Ceder, G.; Persson, K. A. The Materials Application Programming Interface (API): A simple, flexible and efficient API for materials data based on REpresentational State Transfer (REST) principles. *Comput. Mater. Sci.* **2015**, *97*, 209−215.

(65) Suzuki, T.; Nomura, T.; Kuroha, T.; Miyata, N.; Tamura, S.; Tokuhiro, K.; Hato, K. Niobium nitride and method for producing same, niobium nitride-containing film and method for producing same, semiconductor, semiconductor device, photocatalyst, hydrogen generation device, and energy system. U.S. Patent No. 9,114,379, 25 Aug, 2015.

(66) Bailey, E.; Ray, N. M.; Hector, A. L.; Crozier, P.; Petuskey, W. T.; McMillan, P. F. Mechanical properties of titanium nitride nanocomposites produced by chemical precursor synthesis followed by high-p, t treatment. *Materials* **2011**, *4*, 1747−1762.

(67) Ching, W. Y.; Mo, S. D.; Ouyang, L.; Tanaka, I.; Yoshiya, M. Prediction of the new spinel phase of Ti 3 N 4 and SiTi 2 N 4 and the metal-insulator transition. *Phys. Rev. B: Condens. Matter Mater. Phys.* **2000**, *61*, 10609.

(68) Xu, M.; Wang, S.; Yin, G.; Li, J.; Zheng, Y.; Chen, L.; Jia, Y. Optical properties of cubic Ti3N4, Zr3N4, and Hf3N4. *Appl. Phys. Lett.* **2006**, *89*, 151908−151908.

(69) Christensen, A. N.; et al. A neutron diffraction investigation on single crystals of titanium carbide, titanium nitride, and zirconium nitride. *Acta Chem. Scand.* **1975**, *29*, 563−568.

(70) Bhadram, V. S.; Kim, D. Y.; Strobel, T. A. High-pressure synthesis and characterization of incompressible titanium pernitride. *Chem. Mater.* **2016**, *28*, 1616−1620.

(71) Friedrich, A.; Winkler, B.; Bayarjargal, L.; Morgenroth, W.; Juarez-Arellano, E. A.; Milman, V.; Refson, K.; Kunz, M.; Chen, K. Novel rhenium nitrides. *Phys. Rev. Lett.* **2010**, *105*, 085504.

(72) Zhang, R. F.; Lin, Z. J.; Mao, H. K.; Zhao, Y. Thermodynamic stability and unusual strength of ultra-incompressible rhenium nitrides. *Phys. Rev. B: Condens. Matter Mater. Phys.* **2011**, *83*, 060101.

(73) Kawamura, F.; Yusa, H.; Taniguchi, T. Synthesis of rhenium nitride crystals with MoS2 structure. *Appl. Phys. Lett.* **2012**, *100*, 251910.

(74) Wang, Y.; Yao, T.; Yao, J. L.; Zhang, J.; Gou, H. Does the real ReN 2 have the MoS 2 structure? *Phys. Chem. Chem. Phys.* **2013**, *15*, 183−187.

(75) Coy, N. H.; Sponer, H. Emission Spectrum of Antimony Nitride. *Phys. Rev.* **1940**, *58*, 709.

(76) Sun, Q.; Li, W. J.; Fu, Z. W. A novel anode material of antimony nitride for rechargeable lithium batteries. *Solid State Sci.* **2010**, *12*, 397−403.

(77) Schurman, I.; Fernelius, W. C. Nitridation Studies. I. Introduction. II. Mercuric Nitride and Bismuth Nitride as Nitridizing Agents. *J. Am. Chem. Soc.* **1930**, *52*, 2425−2430.

(78) Wang, S. M.; Ge, H.; Sun, S. L.; Zhang, J. Z.; Liu, F. M.; Wen, X. D.; Yu, X. H.; Wang, L. P.; Zhang, Y.; Xu, H. W.; et al. A New Molybdenum Nitride Catalyst with Rhombohedral MoS2 Structure for Hydrogenation Applications. *J. Am. Chem. Soc.* **2015**, *137*, 4815−4822.

(79) Yu, S.; Huang, B.; Jia, X.; Zeng, Q.; Oganov, A. R.; Zhang, L.; Frapper, G. Exploring the Real Ground-State Structures of Molybdenum Dinitride. *J. Phys. Chem. C* **2016**, *120*, 11060−11067.

(80) Schneider, S. B.; Frankovsky, R.; Schnick, W. Synthesis of Alkaline Earth Diazenides MAEN2 (MAE= Ca, Sr, Ba) by Controlled Thermal Decomposition of Azides under High Pressure. *Inorg. Chem.* **2012**, *51*, 2366−2373.

(81) Gregoryanz, E.; Sanloup, C.; Somayazulu, M.; Badro, J.; Fiquet, G.; Mao, H. K.; Hemley, R. J. Synthesis and characterization of a binary noble metal nitride. *Nat. Mater.* **2004**, *3*, 294−294.

(82) Young, A. F.; Sanloup, C.; Gregoryanz, E.; Scandolo, S.; Hemley, R. J.; Mao, H. K. Synthesis of novel transition metal nitrides IrN 2 and OsN 2. *Phys. Rev. Lett.* **2006**, *96*, 155501.

(83) Crowhurst, J. C.; Goncharov, A. F.; Sadigh, B.; Evans, C. L.; Morrall, P. G.; Ferreira, J. L.; Nelson, A. J. Synthesis and characterization of the nitrides of platinum and iridium. *Science* **2006**, *311*, 1275.

(84) Yu, R.; Zhang, X. F. 2005. Platinum nitride with fluorite structure. *Appl. Phys. Lett.* **2005**, *86*, 121913.

(85) Crowhurst, J. C.; Goncharov, A. F.; Sadigh, B.; Zaug, J. M.; Aberg, D.; Meng, Y.; Prakapenka, V. B. Synthesis and characterization of nitrides of iridium and palladium. *J. Mater. Res.* **2008**, *23*, 1−5.

(86) Kawamura, F.; Yusa, H.; Taniguchi, T. Synthesis of rhenium nitride crystals with MoS2 structure. *Appl. Phys. Lett.* **2012**, *100*, 251910.

(87) Niwa, K.; Suzuki, K.; Muto, S.; Tatsumi, K.; Soda, K.; Kikegawa, T.; Hasegawa, M. Discovery of the Last Remaining Binary Platinum-Group Pernitride RuN2. *Chem. - Eur. J.* **2014**, *20*, 13885−13888.

(88) Young, A. F.; Sanloup, C.; Gregoryanz, E.; Scandolo, S.; Hemley, R. J.; Mao, H. K. Synthesis of novel transition metal nitrides IrN2 and OsN2. *Phys. Rev. Lett.* **2006**, *96*, 155501.

(89) Kulkarni, A.; Schön, J. C.; Doll, K.; Jansen, M. Structure prediction of binary pernitride MN2 compounds (M= Ca, Sr, Ba, La, and Ti). *Chem. - Asian J.* **2013**, *8*, 743−754.

(90) Yu, S.; Zeng, Q.; Oganov, A. R.; Frapper, G.; Zhang, L. Phase stability, chemical bonding and mechanical properties of titanium nitrides: a first-principles study. *Phys. Chem. Chem. Phys.* **2015**, *17*, 11763−11769.

(91) Wessel, M.; Dronskowski, R. A New Phase in the Binary Iron Nitrogen System?—The Prediction of Iron Pernitride, FeN2. *Chem. - Eur. J.* **2011**, *17*, 2598−2603.

(92) Kang, S.; Mo, Y.; Ong, S. P.; Ceder, G. A facile mechanism for recharging Li2O2 in Li−O2 batteries. *Chem. Mater.* **2013**, *25*, 3328−3336.